water

MDPI

Article

Preparation of Porous Carbon Materials as Adsorbent Materials from Phosphorus-Doped Watermelon Rind

Yumeng Wei [1], Penghui Li [1,2], Chi Yang [1], Xiaoyu Li [1], Dairenjie Yi [1] and Wenjuan Wu [1,2,*]

[1] College of Light Industry and Food Engineering, Nanjing Forestry University, Nanjing 210037, China; yyqx@njfu.edu.cn (Y.W.); liph@njfu.edu.cn (P.L.); flipped@njfu.edu.cn (C.Y.); lixiaoyu@njfu.edu.cn (X.L.); 359501954@njfu.edu.cn (D.Y.)

[2] Jiangsu Co-Innovation Center of Efficient Processing and Utilization of Forest Resources, Nanjing Forestry University, Nanjing 210037, China

* Correspondence: wenjuanwu@njfu.edu.cn; Tel.: +86-025-8542-7643

Abstract: In this study, phosphorus-doped watermelon rind carbon material (WC-M) was prepared by a muffle furnace, and the adsorption performance of WC-M material to dyes was investigated. At the same time, the effects of dye concentration, pH, adsorption time, adsorption temperature, and other factors on the adsorption effect were investigated. In the experiment, a muffle furnace was used to carbonize the watermelon rind doped with phosphoric acid, which simplified the experimental operation. Regarding the results of SEM analysis, the surface structure of WC-M materials is diverse. Isothermal maps of nitrogen adsorption and desorption show that the material contains more microporous structures and exhibits more active sites. The experimental results show that WC-M materials show good adsorption properties against cationic dyes (malachite green, MG) and anionic dyes (active black, AB). The neutral condition is conducive to the adsorption of MG, and the alkaline condition is conducive to the adsorption of AB. The adsorption rate reaches a maximum in the initial stage of adsorption, the adsorption capacity reaches 50% of the total adsorption capacity within 10 minutes before the reaction, and then the adsorption capacity gradually decreases until the adsorption equilibrium. The adsorption mechanism was explored by the pseudo-first-order kinetic model, second-order kinetic model, and intraparticle diffusion model. At the same time, through the analysis of multiple isotherm models, the overall adsorption process followed the Langmuir isotherm model, the adsorption of MG was more inclined to monolayer electron adsorption, and the adsorption capacity reached 182.68 $mg \cdot g^{-1}$. The reusability of WC-M materials in MG and AB adsorption was discussed. At this time, the concentrations of AB and MG were 120 $mg \cdot L^{-1}$ and 150 $mg \cdot L^{-1}$, and after 10 h of desorption, the desorption rates of MG and AB reached 67.7% and 83.3%, respectively; after five adsorption–desorption cycles, the adsorption rate of MG was still 78.5%, indicating that WC-M materials have good recovery effect. At the same time, the use of watermelon rind as an adsorption material belongs to the high-value application of watermelon rind, which belongs to "turning waste into treasure" and will not pose a certain threat to the environment. This experiment is also suitable for durian rind, pineapple rind, and other "waste" biomass materials, and the experiment has certain generalizations.

Keywords: watermelon rind; carbon material; adsorption; biomass; malachite green; active black

check for updates

Citation: Wei, Y.; Li, P.; Yang, C.; Li, X.; Yi, D.; Wu, W. Preparation of Porous Carbon Materials as Adsorbent Materials from Phosphorus-Doped Watermelon Rind. *Water* **2023**, *15*, 2433. https://doi.org/10.3390/w15132433

Academic Editors: Ali Ayati and Bahareh Tanhaei

Received: 11 May 2023
Revised: 11 June 2023
Accepted: 26 June 2023
Published: 30 June 2023

Copyright: © 2023 by the authors. Licensee MDPI, Basel, Switzerland. This article is an open access article distributed under the terms and conditions of the Creative Commons Attribution (CC BY) license (https://creativecommons.org/licenses/by/4.0/).

1. Introduction

The first synthetic dye was born in 1856, and to date, more than 100,000 dyes have been synthesized and produced worldwide [1]. Dyes are widely used in printing, textile, and other industries [2], and the application is developing rapidly. However, due to the poor dye dyeing process at present, 10% to 15% of the dye in the production will directly enter the production wastewater [1], which is discharged with the factory sewage, causing serious environmental pollution. Due to the complex structure of the dye, it is difficult

to carry out decolorization treatment. Most dyes are mutagenic and carcinogenic due to the aromatic rings they contain [3], so how to remove dyes from wastewater has become a topic of widespread concern. In the process of treating dyes, many treatment methods, such as the oxidation process [4], electrocoagulation technology [5], and adsorption [6], have appeared, but due to their limitations, they are not suitable for large-scale sewage treatment [3]. Due to their high specific surface area, large pore volume, rich pore structure, and adjustable surface chemistry, carbon materials have become one of the most important adsorption materials [7]. Although commonly used carbon materials can achieve good adsorption performance after modification and other treatments [8], because commonly used carbon materials are usually derived from non-renewable fossil fuel resources, such as oil and coal [9], and the cost of synthesis is high [10], the search for renewable and effective carbon adsorption materials with low synthesis cost has become an urgent need.

In recent years, biomass carbon materials have attracted widespread attention because their adsorption capacity is comparable or even better than that of commonly used carbon materials [11], as well as their ability to reduce costs [12] and protect the environment [13]. Biomass is a naturally occurring non-fossil-based organic material with the potential to be a good alternative to fossil fuels [14]. Its main sources are by-products of agricultural, forestry, and municipal waste, which come from a wide range of sources and varieties [15]. Biomass can be processed into benzene and phenol and their derivatives, ethanol, biochar, coke, and other products, with numerous processing methods [16]. The diversity of the two makes it possible to enrich the carbon structure of biomass carbon materials and their wide application [17]. Among them, the biomass production of carbon materials has a long history [18], and with the development of new carbon-based nanomaterials, biomass-derived carbon material nanomaterials have attracted much attention in many potential fields because of their high specific surface area, adjustable structure, low toxicity, long life, and other excellent properties, which has improved the value of biomass utilization [19]. Biomass carbon materials are often used as adsorption materials due to their simple preparation methods, low cost, large specific surface area, and porous structure [20]. At present, the raw materials used to make carbon materials for biomass adsorption include flowers [21], fruits, agricultural product wastes [12], etc. Lu et al. [22] synthesized NaOH-KR by chemical modification of kangkong root (KR) with NaOH for the removal of methyl violet dye. The maximum adsorption capacity of NaOH-KR adsorbent was predicted to be 551.5 $mg \cdot g^{-1}$ by the Sips model, and the maximum adsorption capacity of unmodified KR was increased by 55%. Suhaimi et al. [23] generated biochar by pyrolysis of bamboo at different temperatures (400–800 °C) and found that the temperature of pyrolysis significantly affected the generated biochar's performance. Among them, the best adsorption performance of biochar was obtained by pyrolysis at 500°C, and the maximum adsorption capacity of 86.6 $mg \cdot g^{-1}$ was obtained by the Langmuir model. Hung et al. [24] prepared activated carbon from longan seeds by two-step pyrolysis for the adsorption of methylene blue and methyl orange dyes. The maximum adsorption capacities of 502.84 $mg \cdot g^{-1}$ and 397.77 $mg \cdot g^{-1}$ were obtained by the Langmuir isotherm model, respectively. Kumari [25] et al. used linseed oil as a carbon source to synthesize carbon nano ionic materials (CNOs) with hydrophobic and lipophilic properties. CNOs were used to remove organic solvents and oil from oil–water organic solvents, and oil from the mixture showed high adsorption efficiency and good adsorption of organic solvents such as dichloromethane, chloroform, and toluene.

According to the ATLASBIG database, the world produces about 117,204,081 tons of watermelons per year, of which China is the world's largest producer of watermelons with an annual output of about 79,244,271 tons and a per capita output of about 56 kg. Under the huge data of watermelon production, there is a major problem of environmental pollution caused by discarding watermelon rind. Watermelon rind is mostly used as agricultural waste, such as fertilizer and animal feed for low-value uses [26], and to a lesser extent as food (watermelon paste). How to realize the high-value utilization of watermelon rind and turn waste into treasure has become a problem that people think

about. Watermelon rind can be considered a potential carbon precursor due to its rich content of organic and inorganic substances, such as gum, cellulose, amino acids, etc. [27]. The value of watermelon rind carbon materials as catalysts [27,28], aerogels [29], electrode capacitor materials [30,31], and other aspects are also gradually being explored. At the same time, watermelon rind carbon material can also be used as an adsorption material. Üner et al. [32] demonstrated that the biowaste watermelon rind activated carbon prepared using zinc chloride with an impregnation ratio of 1/600 at 3 °C has the highest mesoporous volume of 1.41 $cm^3 \cdot g^{-1}$, which can be used to adsorb large volume molecules such as dyes. Moreno-Barbosa et al. [33] synthesized watermelon rind activated carbon by phosphoric acid chemical activation of 40% *w*/*w*, which adsorbed lead and zinc in water, and experiments showed that the watermelon rind carbon material had pores and a large specific surface area, which could effectively adsorb lead and zinc. Gupta et al. [34] used a watermelon rind carbon-based adsorbent to adsorb copper dissolved in aqueous solution in the presence of ultrasonic waves. It was found that the degree of adsorption increased with the decrease of the initial concentration and particle size and the increase of ultrasonic power until the optimal state was reached. The maximum adsorption capacity of calcium hydroxide-treated watermelon is 31.25 $mg \cdot g^{-1}$, and the maximum adsorption capacity of citric acid-treated watermelon is 27.027 $mg \cdot g^{-1}$, which can effectively achieve the purpose of removing copper from aqueous solution. This experiment is committed to the development of green and renewable "waste" watermelon rind biomass material and its simple chemical modification, so that it can effectively remove malachite green (MG) and active black (AB) dyes; improve the use value of biomass materials; and achieve the purpose of energy saving, environmental protection, and coordinated development. The phosphorus-doped watermelon rind porous carbon material (WC-M) was prepared in the experiment by adopting a muffle furnace, and the surface characteristics and adsorption properties of WC-M material were investigated. Meanwhile, the effects of dye concentration, pH value, adsorption time, and adsorption temperature on the adsorption effect of WC-M materials were investigated.

2. Materials and Methods

2.1. Materials and Reagents

The raw material for watermelon rinds comes from large farmers markets in Jiangsu Province, China, and is the waste of watermelon products sold in the market. The watermelon rind is treated to remove the outermost hard green peel, leaving a tender green color and an unconsumed white watermelon rind. Put the watermelon rind in boiling hot water, soak, allow the water to cool, and wash and remove the rind. Place it in an oven at 105 °C for 72 h to get dried watermelon rind. Crush the dried watermelon to get a dry powder of the watermelon rind.

The deionized water comes from the laboratory of Nanjing Forestry University in Jiangsu Province, China. The sodium hydroxide and hydrochloric acid used in the experiment came from Sinopharm Chemical Reagent Co., Ltd, No.123 Fuzhou Road, Huangpu District, Shanghai, China. Absolute ethanol and the dyes MG and AB used in the experiment came from Nanjing Chemical Reagent Co., Ltd. in Nanjing, China (for specific information on the dyes, see Table S1).

2.2. Preparation Method

Preparation of watermelon rind porous carbon material doped with phosphorus by muffle furnace was conducted. First, 10 g of prepared dried watermelon rind powder was weighed and evenly mixed with 12 mL of phosphoric acid at a concentration of 17.24 $mol \cdot L^{-1}$, so that the mass ratio of dried watermelon rind powder to phosphoric acid was kept at 1:2 to obtain the turbid solution. Secondly, the prepared turbid samples were carbonized in a muffle furnace at a heating rate of 10 $°C \cdot min^{-1}$, with the turbid samples in an air-tight environment: Place the samples in a clean crucible, place in a muffle furnace, set the heating temperature to 700 °C, and set the heating time to 2 h. Cool to room

temperature, take out the prepared product, wash the prepared product with deionized water several times, and continue to dry in a 105 °C oven for 6 h to obtain WC-M material. The process of WC-M material preparation is shown in Figure 1.

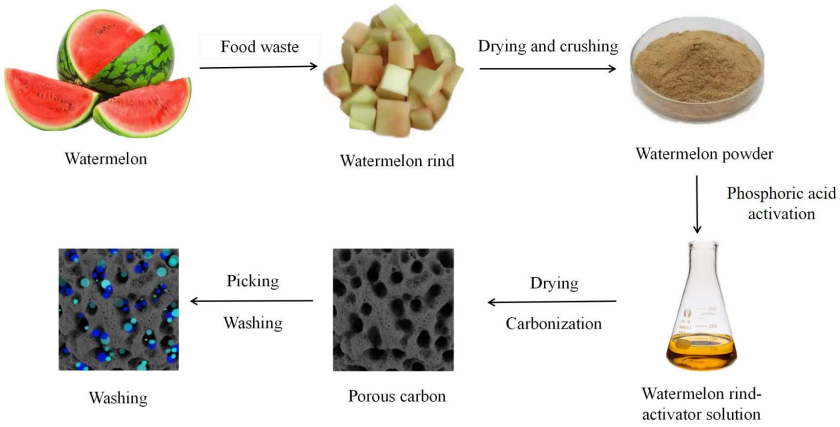


Figure 1. WC-M material preparation process.

2.3. Analysis Method

2.3.1. Scanning Electron Microscopy Test Analysis

The Quanta 20-field emission scanning electron microscope of Hitachi Company of Japan was selected to observe the microscopic morphological characteristics of WC-M materials. Before SEM test, the material sample needs to be processed, first the material is ground into powder, and then the WC-M material sample adheres to the conductive colloid of the sample stage, and the sample is sprayed with gold to eliminate the electrostatic influence between the samples in the reaction.

2.3.2. FTIR Spectrum

The sample was selected to be measured by the KBr compression method in the wavelength range of 4000–400 cm^{-1} using a German model VERTEX 80 V infrared spectrometer.

2.3.3. Analysis of Nitrogen Adsorption–Desorption Curve

Firstly, the specific surface area, pore volume, and distribution of the WC-M material were analyzed by using the American company QUADRASORB-EVO gas adsorber, and then the above pore structure parameters were calculated by the analysis of BET curve. About the sample preparation method: Firstly, 150 °C was selected as the reaction temperature of the pretreatment, and the sample was pretreated for 8 h. After the pretreatment, a series of automatic physicochemical adsorption instruments were used to test the adsorption and desorption process of WC-M samples. Regarding the method of obtaining the calculation results: the specific surface area of the prepared carbon material was calculated by the multi-point method (Brunauer–Emmett–Teller, BET), and the pores of the material were calculated by the Barrett–Joyner–Halenda (BJH) method.

2.3.4. Raman Spectroscopy

The DXR532 laser Raman spectrometer of Themor (Instruments from Thermo Fisher Scientific, Waltham, MA, USA) was selected to analyze the graphitization degree of the sample. Regarding the sample preparation: Place the sample on the sample holder to ensure that the sample is as flat and smooth as possible. After that, according to the characteristics of the sample and experimental requirements, select the appropriate laser wavelength, power and detector, and other parameters. In this experiment, the laser power is selected as 0.1 mW, and the exposure time is selected as 10 s. Raman spectroscopy of WC-M samples was selected under 532 nm photoexcitation (Instruments from Thermo Fisher Scientific, Waltham, Massachusetts, USA).

3. Results and Discussion

3.1. Characterization of WC-M Materials

The surface topography of the sample directly affects the adsorption characteristics [35], so the surface topography of the material can be analyzed by electron microscopy scanning in Figure 2 to analyze its adsorption performance. According to Figure 2a,b, it can be seen that the surface of the untreated watermelon rind has less pore size and the material surface is relatively flat. According to Figure 2c,d, it can be seen that, after high-temperature carbonization, the WC-M material consists of more inhomogeneous size of blocky interconnected carbon structures with the particle size range maintained at around 10–30 μm, and with the decrease of carbon structure size, the roughness of the particle surface increases and more porous structures appear, indicating that it has the characteristics of diversified surface structure, which is conducive to the diffusion of ions in the reaction and makes the material better adsorb dye molecules.

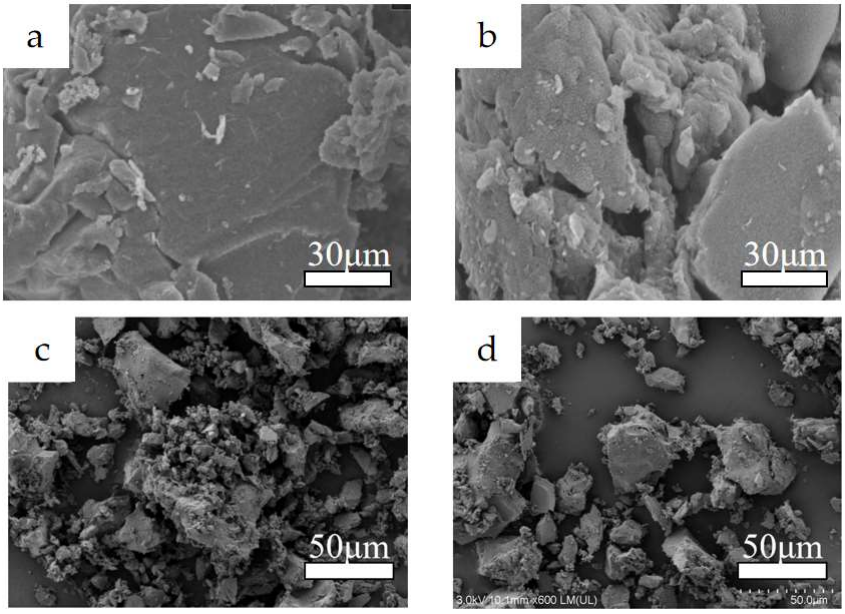


Figure 2. (**a**,**b**) Electron microscopic scans showing watermelon rinds and (**c**,**d**) showing electron microscopic scans of prepared WC-M materials.

The FTIR spectroscopy technique can serve to identify the functional groups that interact with the dye ions in the solution [36]. Figure 3 shows the changes in the FTIR spectra of the WC-M material before and after the adsorption of AB and MG dyes. It can be seen that the broader absorption band observed between 3250 and 3500 cm^{-1} corresponds to the stretching vibration of -OH, and the asymmetry and position of this -OH band at lower wave numbers indicate the presence of strong hydrogen bonds [37]. The two smaller absorption peaks at 2920 cm^{-1} and 2870 cm^{-1} correspond to the stretching vibrations of alkyl, methyl, methylene, or methoxy-CH groups. The stretching vibrations appearing between 1600 and 1720 cm^{-1} appear in the -C=O stretching peak of WC-M. The FTIR spectrum of the WC-M material changed significantly after binding with the dye molecule, with a shift in position and a decrease in intensity in the -OH band. In addition, the disappearance of the -C=O absorption peak was observed in WC-M-MG [37], which suggests that it may act as an adsorption site for MG binding.

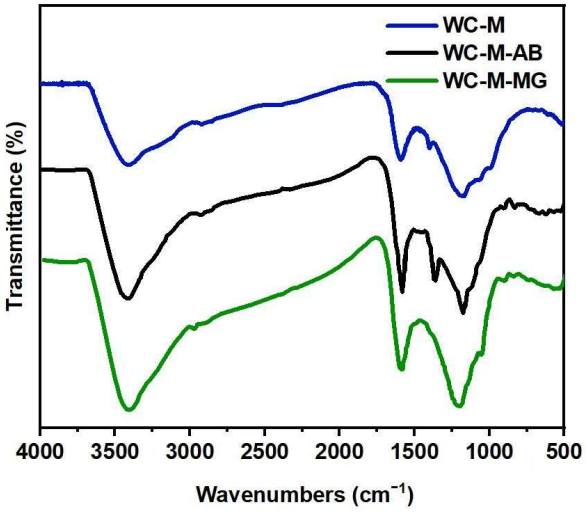


Figure 3. FTIR spectroscopy of WC−M.

3.2. Thermodynamic and Kinetic Analysis of WC-M Material Adsorption

Figure 4 shows the isothermal diagram of the nitrogen adsorption–desorption curve of WC-M materials. As shown in Figure 4, type IV(a) isotherms (according to IUPAC classification) are presented [38], and no obvious saturated adsorption platform appears, indicating that the structure of the pores in the WC-M material is irregular. At the same time, the hole is a gap hole, which is mainly composed of micropores and middle holes. Combined with the pore distribution polyline, it can be seen that there are more microporous structures and fewer mesoporous structures in WC-M materials, and the average pore size of WC-M samples is calculated by BJH method to be 2.98 nm, and the pore volume is 0.24 $cm^3 \cdot g^{-1}$, which is conducive to the display of more active sites in the material. In addition, the specific surface area of WC-M materials is calculated by the BET method, and the specific surface area of WC-M is 358.34 $m^2 g^{-1}$.

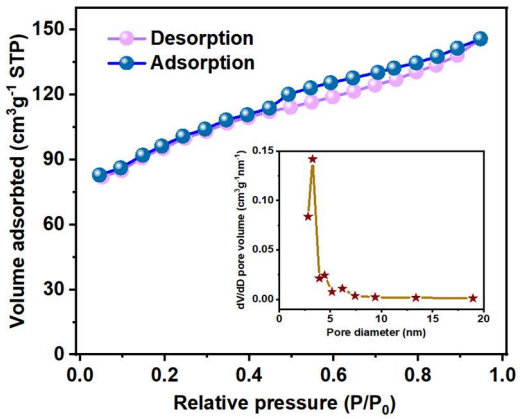


Figure 4. N_2 adsorption−desorption curve and pore size distribution of WC−M materials.

In adsorption experiments on solutions, an important parameter that affects the results of adsorption experiments is the pH of the solution [39]. pH affects not only the activity of functional groups on the surface of biomass, but also the availability of dye molecules in biomass adsorption [40]. The effect of pH on the adsorption of MG and AB in WC-M materials was investigated, and pH was used as the only variable condition for the experiments. The pH values were 3, 4, 5, 6, 7, and 8. According to Figure 5, for MG dye solutions, the adsorption capacity increased with pH at pH < 6. The WC-M materials had a strong pH dependence on the MG adsorption process at this stage. When pH > 6, the adsorption capacity decreased with the increase in pH. When pH = 6, the adsorption

amount reached the maximum value of 191.34 mg·g^{-1}. In the adsorption process, the effect of pH on the adsorption of MG may be related to the surface functional group activity of the prepared material WC-M, and OH^- or H^+ may have some effect on the adsorption of MG. For the AB dye solution, the overall adsorption process of WC-M showed a certain dependence on the pH value, and its adsorption capacity showed an increasing trend with the increase of pH value, and the adsorption amount was 81.68 mg·g^{-1} when the pH value was 8. This result indicated that when the adsorbent dosage and experimental temperature were kept at a certain level, keeping the MG solution in a neutral state and the AB solution in a more basic state. The adsorption capacity of WC-M on MG dye solution and AB dye molecules was improved.

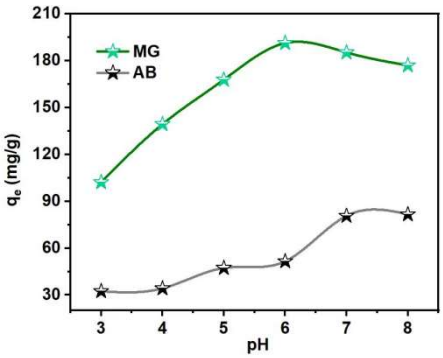


Figure 5. The equilibrium concentration of adsorbed dye changes with pH.

By changing the ambient environment temperature for an adsorption experiment, the effect on the efficiency of the adsorption experiment by temperature was discussed. Figure 6a,b shows the adsorption capacity of WC-M material for MG and AB dyes at various frequencies. The sorption capacity analysis in the figure shows that the sorption capacity of both MG and AB decreases with increasing sorption temperature. The decline in adsorption ability with increased temperature could be attributed to the decrease in the surface activity of the WC-M material due to the increase in temperature [41].

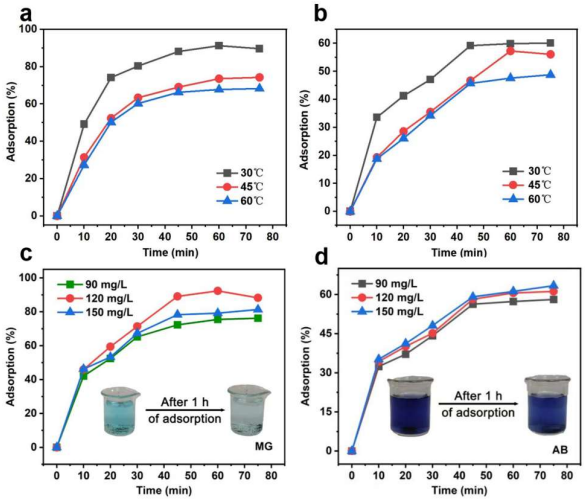


Figure 6. (**a**) Variation of MG adsorption capacity with time at different temperatures. (**b**) Variation of AB adsorption capacity with time at different temperatures. (**c**) Variation of MG adsorption capacity with time at different concentrations. (**d**) Variation of AB adsorption capacity with time at different concentrations.

The adsorption capacity of WC-M materials for MG and AB solutions is affected by time and concentration, as shown in Figure 6c,d. The figure shows the change of the adsorption percentage of WC-M material to different concentrations (90 mg·L^{-1}, 120 mg·L^{-1},

150 mg·L^{-1}) of dye solution with time, and it could be observed that the percentage of adsorption changed over time. The initial WC-M material has a high adsorption rate for MG and AB dyes, and the adsorption percentage for MG and AB accounts for about 50% of the total adsorption percentage in the first 10 min of adsorption; then, the adsorption rate gradually decreases and gradually reaches the saturation state of adsorption after 45 min. The faster initial adsorption rate is due to the high initial phase gradient of concentration in the liquid, when there are more binding active sites in the biomass, and the decrease in the concentration gradient and the decrease in active sites with time leads to a decrease in the adsorption rate [42].

The relationship between specific adsorption rate and adsorption time was explored by adsorption kinetics. The greater the sorption efficiency, the less time is required for the sorption to reach the maximum sorption capacity [43]. According to the above analysis, the adsorption effect of WC-M on MG is obvious, and the adsorption effect on AB is small; this may be due to the fact that the adsorption of MG and AB is a chemisorption process resulting from the interaction of the cationic groups in MG and AB with the anionic groups in WC-M, which has highly preferred adsorption capacity for various cationic dyes [44]. So, in the following analysis, MG is selected for further exploration. Here, pseudo-first-order kinetic models, second-order kinetic models, and intraparticle diffusion models are used to explore them.

Pseudo-first-order kinetic model as follows

$$\log(q_e - q_t) = \log q_e - \frac{k_1 t}{2.303} \quad (1)$$

where q_e is the equilibrium adsorption capacity, and the unit is mg·g^{-1}; k_1 is the adsorption rate constant of the pseudo-first-level model, and the unit is min^{-1}; and q_t is the adsorption capacity in t time, and the unit is mg·g^{-1}.

Pseudo-second-order kinetic model as follows

$$\frac{t}{q_t} = \frac{1}{k_2 q_e^2} + \frac{t}{q_e} \quad (2)$$

In the formula, k_2 is the adsorption rate constant of the pseudo-second-order model, and the unit is g(mg·min)$^{-1}$; q_t is the adsorption amount of the adsorbent with unit mass at any adsorption time, and the unit is mg·g^{-1}.

The associated factors of the pseudo-first-order and pseudo-second-order models calculated with the regression equations of MG adsorption are shown in Table 1, and the linear relationship plots are shown in Figure 7a,b. According to the calculated results, the related factor R^2 for the pseudo-second-order kinetic equation of MG is higher than the pseudo-first-order correlation coefficient, and the fitting effect is better, so the adsorption of MG on WC-M materials can be described as pseudo-second-order kinetics [45], according to which it can be inferred that, in the adsorption process of the two, chemisorption and physical adsorption coexist and chemisorption dominates.

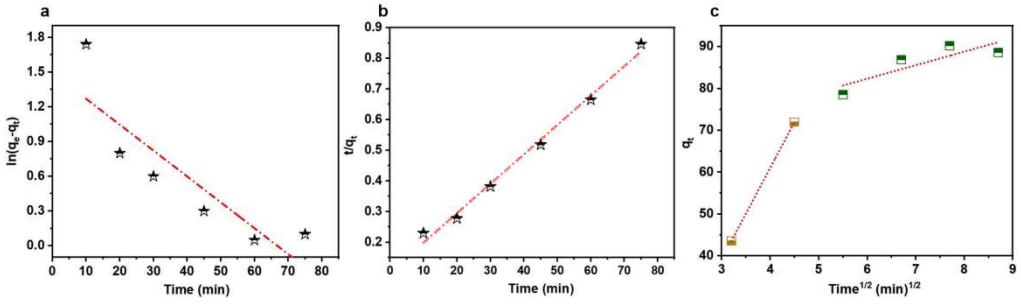


Figure 7. (**a**) Pseudo-first-order kinetic model of MG adsorption by WC−M material. (**b**) Pseudo-second-order kinetic model of MG adsorption by WC−M material. (**c**) Intraparticle diffusion model.

Table 1. Adsorption kinetics constant and parameter values.

Pseudo-First-Order	MG	Pseudo-Second-Order	MG
k_1	3.12	k_2	0.0534
q_e	4.45	q_e	104.28
R^2	0.769	R^2	0.995

Intraparticle diffusion model

$$q_t = k_i t^{1/2} + c_i \quad (3)$$

where k_i is the Webb–Morris adsorption rate constant in $mg(g \cdot min^{1/2})^{-1}$, and q_t is the adsorption capacity of the adsorbent per unit mass at any adsorption time in $mg \cdot g^{-1}$.

The intraparticle diffusion model helps to explore the mechanism of adsorption (Figure 7c). According to Figure 7c, it is clear that the adsorption mechanism can be analyzed in two steps: the first step is the diffusion of MG elements from the aqueous solution to the outer surface of the WC-M material, and the second step is the diffusion of MG elements from the outer surface of the WC-M material to the inner surface of the WC-M material. The first linear stage of the diagram is extended, and the straight line can be represented by the origin as a possible model to explain the current adsorption process.

To further explore the adsorption mechanism of MG dye in WC-M, a variety of isotherms were used to fit it. The Langmuir isotherm model models the correlation with the molecule overprint or adsorption at a certain temperature on a similar solid surface and the air pressure or concentration of the medium above the solid surface, and the Langmuir adsorption isotherm to analyze the results of many adsorption experiments has been used [46].

$$\frac{C_e}{q_e} = \frac{C_e}{q_m} + \frac{1}{bq_m} \quad (4)$$

Among them, q_e and C_e are the adsorption capacity and dye concentration during adsorption equilibrium, and the units are $mg \cdot g^{-1}$ and $mg \cdot L^{-1}$, respectively; q_m is the maximum adsorption capacity of the adsorbent WC-M, and the unit is $mg \cdot g^{-1}$; and b is the affinity-related constant of the binding site in the Langmuir isothermal adsorption model in $L \cdot mg^{-1}$.

The Freundlich isotherm model represents the adsorption capacity on a heterogeneous surface with uniform energy [47]. The Freundlich adsorption model can be represented by Formula (5), where K is the adsorption equilibrium constant of the Freundlich isothermal adsorption model, and the unit is $mg^{1-1/n} \cdot L^{-1/n}$; n is the adsorption intensity constant; and the representation of q_e and C_e can be seen in the formula expression of the Langmuir model above.

$$\ln q_e = \ln K + \frac{\ln C_e}{n} \quad (5)$$

The Temkin isotherm model explores the interaction between WC-M sorbents and MG ions [48]. The Temkin adsorption model can be represented by Equation (6), where B_t can be identified from the slopes of the Temmin isotherm model in Figure 8c, and K_T can be calculated together from the intercept of the slope.

$$q_e = B_t \ln(K_T) + B_t \ln(C_e) \quad (6)$$

The Redlich–Peterson isotherm model is composed of three parameters and can be similarly seen as a combination of the Langmuir and Freundlich isotherms [49]. The rates of β and A can be derived using the slope and intercept from the Redlich–Peterson isotherm model in Figure 8d.

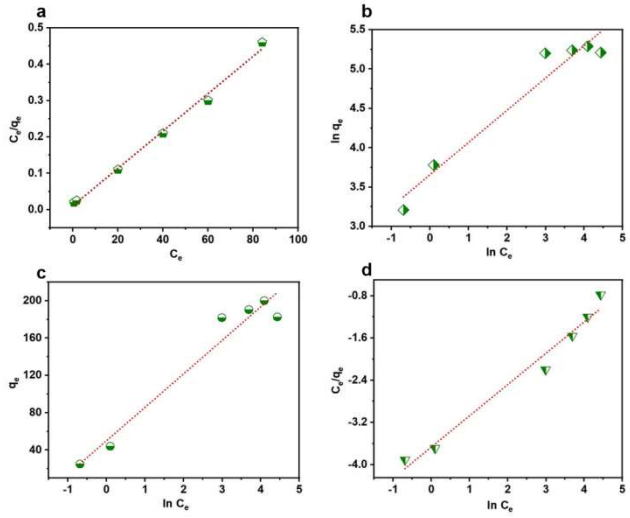


Figure 8. Isotherm models for the adsorption of MG by WC−M materials: (**a**) Langmuir; (**b**) Freundlich; (**c**) Temkin; and (**d**) Redlich–Peterson isotherm models.

$$\ln \frac{C_e}{q_e} = \beta \ln C_e - \ln A \quad (7)$$

The calibration curve of the four model sorption isotherms is presented in Figure 8, and the values of the constants for each model are shown in Table 2. The analysis and comparison revealed that the relevance coefficient R^2 of the Langmuir isotherm was better than the other three isotherms, indicating at present the adsorption test procedure followed the pattern of the Langmuir isotherm and the fit of both was better. This may be due to the preference of WC-M for monolayer adsorption in MG adsorption. The maximum adsorption capacity of WC-M on MG was 182.68 mg·g^{-1} according to the Langmuir isotherm model, which is at a comparable level compared to the maximum adsorption capacity of other adsorbents (Table 3) and even better than most adsorbents.

Table 2. Langmuir, Freundlich, Temkin, and Freundlich adsorb isotherm constants and parameter values.

Langmuir	MG	Freundlich	MG	Temkin	MG	Redlich-Peterson	MG
q_m	194.553	K	38.815	B_t	35.853	β	0.592
b	0.469	n	2.444	K_T	4.038	A	39.017
R^2	0.997	R^2	0.937	R^2	0.943	R^2	0.970

Table 3. Maximum adsorption capacity of different adsorbents for dyes.

Adsorbent	Dye Adsorbate	Maximum Capacity (mg.g−1)	Reference
Vine stem	Acid red 111	58.82	[50]
Peach endocarp shell	Brilliant green 1	49.61	[51]
Yellow mombin fruit stones (CA)	Dianix® royal blue CC (The version number of the software is origin2019)	147.47	[52]
Sour cherry	Yellow 18	76.318	[46]
Green alga ulva lactuca	Direct Red 23	149.26	[47]
Ricinus communis pericarp	Crystal violet	125.25	[41]
Citrus	Methylene blue	313	[53]
Banana peel-activated	Orange II	333	[54]
Bagasse	Acid blue	391	[55]
Brachychiton populneus fruit shell	Methyl green	67.93	[56]
Watermelon rind	Malachite green	182.68	This study
	Active black	81.68	

The exploration of the desorption process is beneficial for further exploration of the adsorption mechanism and the recovery of dyes and adsorbents. The WC-M materials adsorbed with MG and AB were desorbed under acidic conditions, and the results are shown in Figure 9a. The results showed that the desorption rates of MG and AB increased with time, and the desorption rate of AB was significantly larger than that of MG. This may be due to the fact that initially, the WC-M material is better desorbed because of the less adsorption of AB. Since only the dye under physical adsorption can be separated from the surface of the adsorbent WC-M, it can be concluded that the adsorption of the dye by the WC-M material is involved in the process of chemisorption and physical adsorption. The recovery capacity of the adsorbent was evaluated as shown in Figure 9b. After five cycles, the adsorption capacity of MG dye solution was maintained at 78.5% with a good adsorption effect. The decrease in the adsorption capacity of WC-M for the dye was small. Therefore, the WC-M material can be reused, thus increasing the utilization value of the material.

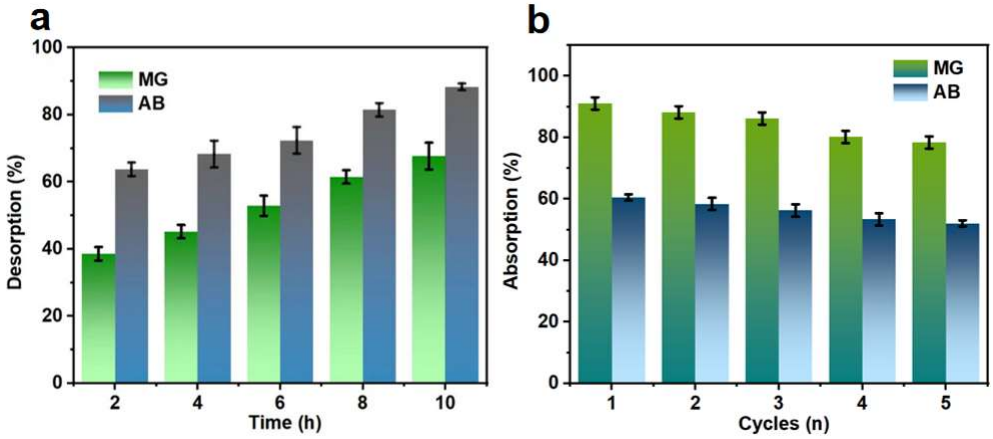


Figure 9. (**a**) Variation of desorption rate of MG and AB adsorbed by WC-M material with time. (**b**) Recyclability of MG and AB adsorbed by WC-M material.

4. Conclusions

This study shows that the prepared WC-M material is an effective adsorbent for removing malachite green dye and active black dye from aqueous solution and has a good adsorption effect. SEM and nitrogen adsorption and desorption isothermal diagrams show that the material contains more microporous structures, which is conducive to the adsorption of dyes. It was found that the adsorption effect was related to pH, temperature, and other factors, and it was easier to be adsorbed when malachite green dye was in a neutral state, and active black dye was easier to be adsorbed in a basic state. By fitting the adsorption kinetic data with the pseudo-first-order kinetics and pseudo-second-order kinetics, the adsorption mechanism was further explored, and it was found that the fitting effect with pseudo-second-order kinetics was better. This shows that in the adsorption of MG by WC-M, chemical adsorption and physical adsorption coexist, and chemical adsorption dominates. The experimental data of MG were fitted by four isotherm models, Langmuir, Freundlich, Temkin, and Redlich–Peterson, among which the Langmuir isotherm fitting effect was better, indicating that WC-M materials were more inclined to monolayer adsorption in the adsorption of MG. The maximum adsorption capacity of WC-M material for MG reached 182.68 $mg \cdot g^{-1}$, and the adsorption performance was better than that of some adsorbents. Finally, the adsorption–desorption process of MG and AB was explored, and WC-M materials had good recyclability. The carbonization of watermelon rind doped with phosphoric acid using a muffle furnace simplifies the experimental process and makes the experiment more convenient. At the same time, the experiment can be generalized to other fruit rinds (durian rinds, pineapple rinds, etc.), which have a certain popularity.

The two make the experiment have certain scientific and educational significance, which is convenient for people to deepen their understanding of the use of biomass carbon materials.

Supplementary Materials: The following supporting information can be downloaded at: https://www.mdpi.com/article/10.3390/w15132433/s1, Figure S1: Basic parameters and fitting standard curve equation of three organic dyes.

Author Contributions: Conceptualization, P.L.; methodology, P.L.; software, Y.W.; validation, Y.W. and C.Y.; investigation, Y.W. and X.L.; resources, Y.W.; data curation, D.Y.; writing—original draft preparation, Y.W.; writing—review and editing, P.L.; supervision, W.W.; project administration, W.W. All authors have read and agreed to the published version of the manuscript.

Funding: This research was funded by National Natural Science Foundation of China, grant number 32271797 and 32201500; Natural Science Foundation of Jiangsu Province, grant number BK20220431; Nanjing Forestry University Undergraduate Innovation Training Program Project (2022NFUSPITP0613).

Data Availability Statement: Not applicable.

Acknowledgments: In addition, Yumeng Wei thanked her supervisor Penghui Li for his patient guidance throughout the experiment and thesis writing.

Conflicts of Interest: The authors declare no conflict of interest.

References

1. Chen, K.C.; Wu, J.Y.; Liou, D.J.; Sz-Chwun, J.H. Decolorization of the textile dyes by newly isolated bacterial strains. *J. Biotechnol.* **2003**, *101*, 57–68. [CrossRef] [PubMed]
2. Susana, R.C. Dye removal by immobilised fungi. *Biotechnol. Adv.* **2009**, *27*, 227–235.
3. Mittal, A.; Mittal, J.; Malviya, A.; Kaur, D.; Gupta, V.K. Adsorption of hazardous dye crystal violet from wastewater by waste materials. *J. Colloid. Interface. Sci.* **2010**, *343*, 463–473. [CrossRef] [PubMed]
4. Belgin, G.; Berkant, K.; Murat, A.G.; Arif, H. Oxidative degradations of reactive blue 4 dye by different advanced oxidation methods. *J. Hazard. Mater.* **2009**, *168*, 129–136.
5. Sittichok, K.; Mail, H. Remediation of wastewater from pulp and paper mill industry by the electrochemical technique. *Chen. Eng. J.* **2009**, *151*, 228–234.
6. Anuradha, N.K.; Umesh, B.J.; Jyoti, P.J.; Vishwas, A.B.; Sanjay, P.G. Biotechnological strategies for phytoremediation of the sulfonated azo dye Direct Red 5B using *Blumea malcolmii* Hook. *Bioresour. Technol.* **2009**, *100*, 4104–4110.
7. Wei, X.; Jiang, X.P.; Liu, X.; Zhou, W.M.; Garba, Z.N.; Lawan, L.; Wang, L.W.; Yuan, Z.H. Adsorption of organic dyes from wastewater by metal-doped porous carbon materials. *J. Clean. Prod.* **2021**, *284*, 124773.
8. Zemskova, L.A.; Voit, A.V.; Sheveleva, I.V.; Mironova, L.N. The sorption properties of chitosan-carbon fibrous materials. *Russ. J. Phys. Chem.* **2007**, *81*, 1658–1661. [CrossRef]
9. Serrano-Ruiz, J.C. Biomass: A renewable source of fuels, chemicals and carbon materials. *Molecules* **2020**, *25*, 5217. [CrossRef]
10. Rezazad, H.; Vahdati-Khajeh, S.; Eftekhari-Sis, B. Egg yolk biomass derived carbon material as a highly efficient and reusable hydrophobic oil-absorbent. *J. Porous Mater.* **2020**, *27*, 1439–1446. [CrossRef]
11. Dai, Y.J.; Mihara, Y.; Tanaka, S.; Watanabe, K.; Terui, N. Nitrobenzene-adsorption capacity of carbon materials released during the combustion of woody biomass. *J. Hazard. Mater.* **2010**, *174*, 776–781. [CrossRef]
12. Quan, G.X.; Yan, J.L.; Ding, C. *Preparation and Characterization of Biomass Carbon Adsorbent from Rice Husk and Its Adsorption Properties on p-Chlorophenol*; Iceesd 2011; Shanghai University of Electric Power: Shanghai, China, 2011; Volume 356–360, pp. 510–513.
13. Jiang, L.L.; Sheng, L.Z.; Fan, Z.J. Biomass-derived carbon materials with structural diversities and their applications in energy storage. *Sci. China Mater.* **2018**, *61*, 133–158. [CrossRef]
14. Mohammed, A.; Lyu, D.M.; Mahtab, N.; Ateeq, S.; Zhou, X.M.; Donald, L.S. Biomass for a sustainable bioeconomy: An overview of world biomass production and utilization. *Renew. Sust. Energ. Rev.* **2021**, *139*, 110691.
15. André, B.; Tim, K.; Jdo, M.; Bernd, M.; Anja, N.; Felix, R.; Thomas, R.; Roland, B.; Thomas, H.; Christian, B.; et al. How to measure the impact of biogenic residues, wastes and by-products: Development of a national resource monitoring based on the example of Germany. *Biomass Bioenergy* **2019**, *127*, 105275.
16. Wang, Z.H.; Shen, D.K.; Wu, C.F.; Gu, H. State-of-the-art on the production and application of carbon nanomaterials from biomass. *Green Chem.* **2018**, *20*, 5031–5057. [CrossRef]
17. Jiang, G.C.; Liu, L.; Xiong, J.J.; Luo, Y.M.; Cai, L.C.; Qian, Y.; Wang, H.; Mu, L.W.; Feng, X.; Lu, X.H.; et al. Advanced material-oriented biomass precise reconstruction: A review on porous carbon with inherited natural structure and created artificial structure by post-treatment. *Macromol. Biosci.* **2022**, *22*, 2100479. [CrossRef]
18. Soumya, R.; Sajini, V. Sustainable carbon nanomaterials: Recent advances and its applications in energy and environmental remediation. *J. Environ. Chem. Eng.* **2016**, *4*, 835–856.
19. Aumber, A.; Lim, T.M.; Anh, N.P. Biomass-waste derived graphene quantum dots and their applications. *Carbon* **2018**, *140*, 77–79.

20. Ding, J.; He, W.Z.; Yu, C.; Liu, Z.L.; Deng, C.J.; Zhu, H.X. Waste biomass derived carbon supported Mo2C/C composite materials for heavy metal adsorption and hydrogen evolution reaction. *Mater. Today Commun.* **2022**, *31*, 103646. [CrossRef]
21. Jia, Z.G.; Li, Z.Y.; Ni, T.; Li, S.B. Adsorption of low-cost absorption materials based on biomass (*Cortaderia selloana* flower spikes) for dye removal: Kinetics, isotherms and thermodynamic studies. *J. Mol. Liq.* **2017**, *229*, 285–292. [CrossRef]
22. Lu, Y.C.; Kooh, M.R.R.; Lim, L.B.L.; Priyantha, N. Effective and simple NaOH-modification method to remove methyl violet dye via lpomoea aquatica roots. *Adsorp. Sci. Technol.* **2021**, *2021*, 5932222. [CrossRef]
23. Suhaimi, N.; Kooh, M.R.R.; Lim, C.M.; Chao, C.T.C.; Chau, Y.F.C.; Mahadi, A.H.; Chiang, H.P.; Hassan, N.H.H.; Thotagamuge, R. The use of gigantochloa bamboo-derived biochar for the removal of mMethylene blue from aqueous solution. *Adsorp. Sci. Technol.* **2022**, *2022*, 8245797.
24. Hung, N.Y.; Nguyet, B.T.M.; Nghi, N.H.; Thanh, N.M.; Quyen, N.D.V.; Nguyen, V.T.; Nhiem, D.N.; Khieu, D.Q. Highly effective adsorption of organic dyes from aqueous solutions on longan seed-derived activated carbon. *Environ. Eng. Res.* **2023**, *28*, 220116. [CrossRef]
25. Kumari, P.; Tripathi, K.M.; Awasthi, K.; Gupta, R. Biomass-derived carbon nano-onions for the effective elimination of organic pollutants and oils from water. *Environ. Sci. Pollut. Res.* **2023**, *30*, 71048–71062. [CrossRef] [PubMed]
26. Ratnakaram, V.N.; Rao, C.G.P.; Sree, S. *Simultaneous Saccharification and Fermentation of Watermelon Waste for Ethanol Production*; Itsfew; Vellore Institute of Technology: Vellore, India, 2018; Volume 2, pp. 196–202.
27. Li, L.; Wu, Z.H.; Zhang, Z.; Zhao, D.Y. Watermelon peel-derived nitrogen-doped porous carbon as a superior oxygen reduction electrocatalyst for zinc-air batteries. *ChemElectroChem* **2021**, *8*, 4790–4796. [CrossRef]
28. Wang, J.M.; Wang, C.W. Watermelon-like metallic Co/graphene-like nanohybrids from electrochemical exfoliation of anthracite coal as superior oxygen reduction reaction electrocatalyst. *ACS Sustain. Chem. Eng.* **2019**, *7*, 12457–12463. [CrossRef]
29. Zhu, B.; Zhao, J.T.; Meng, Y.F.; Liu, Z.X.; Yu, N. Watermelon flesh-derived carbon aerogel with hierarchical porous structure for interfacial solar steam generation. *Sol. Rrl.* **2022**, *6*, 2200270. [CrossRef]
30. Wang, L.; Zhang, L.C.; Cheng, J.X.; Ding, C.X.; Chen, C.H. Watermelon used as a novel carbon source to improve the rate performance of iron oxide electrodes for lithium ion batteries. *Electrochim. Acta* **2013**, *102*, 306–311. [CrossRef]
31. Zhang, P.; Mu, J.H.; Guo, Z.Y.; Wong, S.L. Watermelon peel-derived heteroatom-doped hierarchical porous carbon as a high-performance electrode material for supercapacitors. *ChemElectroChem* **2021**, *8*, 1196–1203. [CrossRef]
32. Üner, O.; Geçgel, Ü.; Bayrak, Y. Preparation and characterization of mesoporous activated carbons from waste watermelon rind by using the chemical activation method with zinc chloride. *Arab. J. Chem.* **2019**, *12*, 3621–3627. [CrossRef]
33. Moreno-Barbosa, J.J.; López-Velandia, C.; Maldonado, A.P. Removal of lead(II) and zinc(II) ions from aqueous solutions by adsorption onto activated carbon synthesized from watermelon shell and walnut shell. *Adsorption* **2013**, *19*, 675–685. [CrossRef]
34. Gupta, H.; Gogate, P.R. Intensified removal of copper from waste water using activated watermelon based biosorbent in the presence of ultrasound. *Ultrason Sonochem.* **2016**, *30*, 116–122. [CrossRef]
35. Anandaraj, B.; Eswaramoorthi, S.; Rajesh, T.P.; Aravind, J.; Babu, P.S. Chromium(VI) adsorption by codium tomentosum: Evidence for adsorption by porous media from sigmoidal dose–response curve. *Int. J. Environ. Sci. Technol.* **2018**, *15*, 2595–2606. [CrossRef]
36. Chigbundu, E.C.; Adebowale, K.O. Equilibrium and fractal-like kinetic studies of the sorption of acid and basic dyes onto watermelon shell (*Citrullus vulgaris*). *Cellulose* **2017**, *24*, 4701–4714. [CrossRef]
37. Husein, D.Z.; Aazam, E.; Battia, M. Adsorption of cadmium(II) onto watermelon rind under microwave radiation and application into surface water from jeddah, saudi arabia. *Arab. J. Sci. Eng.* **2017**, *42*, 2403–2415. [CrossRef]
38. Li, R.S.; Zheng, F.Y.; Zhang, X.H.; Hu, J.D.; Xu, C.Y.; Zhang, Y.C. Phosphorus and iron doped nitrogen-containing carbon derived from biomass for oxygen reduction under various pH conditions. *Int. J. Hydrog. Energ.* **2020**, *45*, 28651–28663. [CrossRef]
39. Binupriya, A.R.; Sathishkumar, M.; Swaminathan, K.; Kuz, C.S.; Yun, S.E. Comparative studies on removal of Congo red by native and modified mycelial pellets of Trametes versicolor in various reactor modes. *Bioresour. Technol.* **2008**, *99*, 1080–1088. [CrossRef]
40. Neeta, A.S. Decolorization of Erythrosine B by Rhizopus arrhizus biomass. *Appl. Water Sci.* **2018**, *8*, 205.
41. Madhavakrishnan, S.; Manickavasagam, K.; Vasanthakumar, R.; Rasappan, K.; Mohanraj, R.; Pattabhi, S. Adsorption of crystal violet dye from aqueous solution using ricinus communis pericarp carbon as an adsorbent. *E-J. Chem.* **2009**, *6*, 1109–1116. [CrossRef]
42. Kannamba, B.; Laxma Reddy, K.; AppaRao, B.V. Removal of Cu(II) from aqueous solutions using chemically modified chitosan. *J. Hazard. Mater.* **2010**, *175*, 939–948. [CrossRef]
43. Zhang, C.; Ren, H.X.; Zhong, C.Q.; Wu, D.J. Biosorption of Cr(VI) by immobilized waste biomass from polyglutamic acid production. *Sci. Rep.* **2020**, *10*, 3075. [CrossRef] [PubMed]
44. Hanafi, N.A.M.; Abdulhameed, A.S.; Jawad, A.H.; ALOthman, Z.A.; Yousef, T.A.; Duaij, O.K.A.; Alsaiari, N.S. Optimized removal process and tailored adsorption mechanism of crystal violet and methylene blue dyes by activated carbon derived from mixed orange peel and watermelon rind using microwave-induced ZnCl2 activation. *Biomass Convers. Biorefin.* **2022**, *14*, 1–13. [CrossRef]
45. Aboua, K.N.; Yobouet, Y.A.; Yao, K.B.; Gone, D.L.; Trokourey, A. Investigation of dye adsorption onto activated carbon from the shells of Macoré fruit. *J. Environ. Manag.* **2015**, *156*, 10–14. [CrossRef] [PubMed]
46. Angin, D. Utilization of activated carbon produced from fruit juice industry solid waste for the adsorption of Yellow 18 from aqueous solutions. *Bioresour. Technol.* **2014**, *168*, 259–266. [CrossRef]

47. El Nemr, A.; Shoaib, A.G.M.; El Sikaily, A.; Safaa; Mohamed, A. E.A.; Hassan, A.F. Utilization of green alga ulva lactuca for sustainable production of meso-micro porous nano activated carbon for adsorption of Direct Red 23 dye from aquatic environment. *Carbon Lett.* **2022**, *32*, 153–168. [CrossRef]
48. Panahi, M.; Behnam, S. Biosorption of Malachite Green dye by the brown alga Dictyota cervicornis: Kinetics and isotherm study. *Color. Technol.* **2018**, *134*, 292–298. [CrossRef]
49. Sharma, G.; Sharma, S.; Kumar, A.; Naushad, M.; Du, B.; Ahamad, T.; Ghfar, A.A.; Alqadami, A.A.; Stadler, F.J. Honeycomb structured activated carbon synthesized from Pinus roxburghii cone as effective bioadsorbent for toxic malachite green dye. *J. Water Process Eng.* **2019**, *32*, 100931. [CrossRef]
50. Ayan, E.M.; Toptas, A.; Kibrislioglu, G.; Yalcinkaya, E.E.S.; Yanik, J. Biosorption of dyes by natural and activated vine stem. Interaction between biosorbent and dye. *Clean* **2011**, *39*, 406–412. [CrossRef]
51. Aguayo-Villarreal, I.A.; Cortes-Arriagada, D.; Rojas-Mayorga, C.K.; Pineda-Urbina, K.; Muniz-Valencia, R.; Gonzalez, J. Importance of the interaction adsorbent-adsorbate in the dyes adsorption process and DFT modeling. *J. Mol. Struct.* **2020**, *1203*, 127398. [CrossRef]
52. Brito, M.J.P.; Veloso, C.M.; Santos, L.S.; Renata, F.B.C.; Fontan, R.D.I. Adsorption of the textile dye Dianix (R) royal blue CC onto carbons obtained from yellow mombin fruit stones and activated with KOH and H_3PO_4: Kinetics, adsorption equilibrium and thermodynamic studies. *Powder Technol.* **2018**, *339*, 334–343. [CrossRef]
53. Koyuncu, F.; Guzel, F. Use of new nanoporous carbon produced from Mandarin (*Citrus reticulata*) industrial processing waste to remove anionic and cationic dyes. *Sep. Sci. Technol.* **2021**, *56*, 1001–1013. [CrossRef]
54. Ma, J.F.; Huang, D.Q.; Zou, J.; Li, L.Y.; Kong, Y.; Komarneni, S. Adsorption of methylene blue and Orange II pollutants on activated carbon prepared from banana peel. *J. Porous Mater.* **2015**, *22*, 301–311. [CrossRef]
55. Valix, M.; Cheung, W.H.; McKay, G. Preparation of activated carbon using low temperature carbonisation and physical activation of high ash raw bagasse for acid dye adsorption. *Chemosphere* **2004**, *56*, 493–501. [CrossRef]
56. Rida, K.; Chaibeddra, K.; Cheraitia, K. Adsorption of cationic dye methyl green from aqueous solution onto activated carbon prepared from BrachychitonPopulneus fruit shell. *Indian J. Chem. Techn.* **2020**, *27*, 51–59.

Disclaimer/Publisher's Note: The statements, opinions and data contained in all publications are solely those of the individual author(s) and contributor(s) and not of MDPI and/or the editor(s). MDPI and/or the editor(s) disclaim responsibility for any injury to people or property resulting from any ideas, methods, instructions or products referred to in the content.